Backbone Flexibility of Five Sites on the Catalytic Subunit of cAMP-Dependent Protein Kinase in the *Open* and *Closed* Conformations†

Milind Gangal,‡ Sarah Cox,§,|| John Lew,§,⊥ Teresa Clifford,§ Siv M. Garrod,§ Melissa Aschbaher,§ Susan S. Taylor,§ and David A. Johnson*,‡

Division of Biomedical Sciences, University of California, Riverside, California 92521-0121, and Department of Chemistry and Biochemistry, School of Medicine, University of California, San Diego, La Jolla, California 92093-0359

Received March 11, 1998; Revised Manuscript Received June 25, 1998

ABSTRACT: To develop an alternative approach to measure peptidyl backbone flexibility and to expand our understanding of the segmental flexibility of cAMP-dependent protein kinase (cAPK), the effect of protein kinase inhibitor peptide, PKIα(5−24), and MgATP on the mobility of fluorescein selectively conjugated to five sites on the catalytic subunit of cAPK was examined. Specifically, five full-length, single-site catalytic subunit mutants (K16C, K81C, I244C, C199A, and N326C) were prepared, and fluorescein maleimide was selectively attached to the side chains of each substituted cysteine or, in the case of the C199A mutant, to the unprotected native C343. The time-resolved anisotropy decay profiles of the five fluorescein maleimide-conjugated mutants were well fit to a biexponential equation. The fast rotational correlation times of the fluorescein conjugates ranged between 1.9 and 2.8 ns and were inversely correlated ($r = -0.87$) to the averaged crystallographic main-chain atom *B* factors around each site of conjugation. The slow correlation times ranged between 25 and 28 ns and were about the same magnitude as the value of 21 ns estimated from the Stokes−Einstein equation. The presence of MgATP and PKIα-(5−24), which induces the *closed* conformation of cAPK, was associated with a reduction of the fast rotational correlation time of the K81C conjugate, indicating that the peptidyl backbone around K81 is measurably less flexible when the C subunit is in the *closed* compared with the *open* conformation. The results suggest (i) that time-resolved fluorescence anisotropy can assess the nanosecond flexibility of short segments of the peptidyl backbone around each site of labeling and (ii) that the substrate/pseudosubstrate binding differentially affects the backbone flexibility of cAPK.

Pseudosubstrate and presumably substrate binding to the catalytic (C) subunit of cAMP-dependent protein kinase (cAPK)[1] in the presence of MgATP induces large-scale structural changes that involve domain displacements and results in the closure of the interdomain cleft that forms the active site (*1*−*3*). These domain displacements are associated with a volume contraction of the C subunit and therefore suggest that some regions of the α-carbonyl backbone should be more flexible than others. What is understood about the peptidyl backbone flexibility of cAPK derives from the analysis of the crystallographic *B* (or temperature) factors of the main-chain atoms. While *B* factors are proportional to the mean-square displacement of the atoms from their rest positions and can vary with vibrational displacement, crystal disorder, and errors in the model, they carry little information on diffusional or vibrational time scales, and the level of molecular dynamics information depends on the resolution of the crystal diffraction pattern.

To begin to develop an alternative approach for the measurement of peptidyl backbone flexibility and to contribute to our understanding of substrate/pseudosubstrate-induced changes in the segmental flexibility of the C subunit in solution, time-resolved fluorescence anisotropy was used to examine the mobility of fluorescein selectively conjugated to five sites on the C subunit of cAPK in the volume-expanded (*open*) and -contracted (*closed*) conformations. Specifically, a panel of four full-length, single-site X-to-Cys mutants and one Cys-to-Ala mutant of the cAPK C subunit were prepared. The four sites of cysteine substitution are illustrated in Figure 1 and include a site on the A helix near the N-terminus (K16C), a site on the B helix near the tip of the small lobe (K81C), a site at the beginning of the G helix near the tip of the large lobe (I244C), and a site on the

† This work was supported by a grant from the National Institutes of Health (NIH GM19301) to S.S.T.

* All correspondence should be addressed to this author at the Division of Biomedical Sciences, University of California, Riverside, CA 92521-0121.

‡ University of California, Riverside.

§ University of California, San Diego.

|| Present address: DuPont Merck Pharmaceutical Co., Experimental Station, E336/36A, Rt. 141 and Henry Clay Rd., Wilmington, DE 19880-0361.

⊥ Present address: Department of Molecular, Cellular, and Developmental Biology, University of California, Santa Barbara, Santa Barbara, CA 93105.

[1] Abbreviations: cAPK, cAMP-dependent protein kinase; buffer A, 30 mM 2-(*N*-morpholino)ethanesulfonic acid, 50 mM NaCl, 1 mM EDTA, 5 mM β-mercaptoethanol, pH 6.5; buffer B, 20 mM KH_2PO_4, 1 mM DTT, pH 6.5; buffer C, 10 mM MOPS, 50 mM KCl, pH 7.2; buffer D, 20 mM MOPS, 50 mM KCl, 5 mM β-mercaptoethanol, pH 7.2; C subunit, the α isoform of the catalytic subunit of cAPK; DTT, dithiothreitol; r_0, time zero anisotropy; r_{VF}, difference between r_0 of immobilized fluorescein (0.34) and the observed r_0; r_F, amplitude of the 'fast' anisotropy decay processes; r_S, amplitude of the 'slow' anisotropy decay processes; ϕ_F, fast rotational correlation time; ϕ_S, slow rotational correlational time.

S0006-2960(98)00560-1 CCC: $15.00
Published on Web 09/09/1998

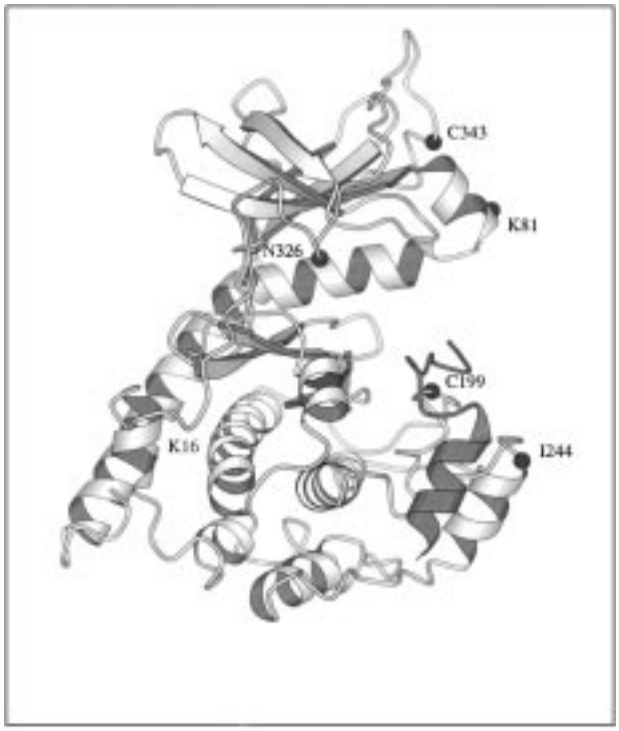

FIGURE 1: Backbone structure of the C subunit of cAPK with sites of X-to-Cys mutation and wild-type cysteines. The positions of the four X-to-Cys mutants are highlighted: K16C (beginning of the A helix), K81C (tip of the small lobe), I244C (tip of the large lobe), and N326C (C-terminal tail). Also highlighted are the two wild-type cysteines, C199 and C343, that were protected from conjugation by the presence of MgATP. Fluorescein maleimide was specifically attached to the side chains of the four X-to-Cys mutants and to C343. The latter site was specifically labeled by using a C199A mutant.

C-terminal tail at the level of the interdomain cleft (N326C). Also illustrated in Figure 1 are the sites of the two native cysteines, C199 and C343, which can be protected from modification with MgATP. The side chains of the substituted cysteines and, in the case of the C199A mutant, the native C343 were selectively conjugated with fluorescein maleimide and the time course of anisotropy decay was measured for each fluorescein conjugate in the absence and presence of the active, truncated form of protein kinase inhibitor peptide, PKIα(5−24), which in the presence of MgATP induces the sustained *closed* conformation of cAPK.

The results show a significant inverse correlation between the relative main-chain atom *B* factors around each site of conjugation and the fast rotational correlational times, suggesting that this approach can monitor peptidyl backbone flexibility of proteins in solution. Also, only the anisotropy decay associated with the K81C mutant conjugate is significantly reduced upon induction of the *closed* conformation, indicating a differentially reduced mobility in the nanosecond time scale of the peptidyl segment around K81C in the *closed* compared with the *open* conformation.

MATERIALS AND METHODS

Preparation and Purification of the Mutant C Subunits. The five mutant C subunits studied (K16C, K81C, I244C, C199A, and N326C) were prepared and purified as described elsewhere (*4*−*6*). Briefly, cDNA corresponding to the wild-type murine C_α subunit was mutated to encode Cys at the four above-mentioned positions or in the case of C199A an alanine. Each mutant was overexpressed in *E. coli* strain BL21-DE3. The bacteria were pelleted, resuspended in buffer A (30 mM MES, 50 mM KCl, 1 mM EDTA, 5 mM β-mercaptoethanol, pH 6.5), and lysed or fractured in a French pressure cell operated between 900 and 1200 psi. The suspension was then centrifuged at 15 000 rpm with a Beckman JA-20 rotor for 40 min. The supernatant was diluted 4-fold with chilled distilled water (conductivity ≤1.2 mS/cm), adjusted to a pH of 6.5, and then incubated with 30 mL of P-11 resin (Whatman) for 2−3 h at 4 °C. After centrifugation (1000*g*), the pelleted resin was washed first with 250 mL and then with 400 mL of buffer A that included 90 mM potassium phosphate (pH 6.5). After placing the washed resin in a column (2.5 × 25 cm), the mutant enzyme was eluted with buffer A plus 250 mM potassium phosphate at a flow rate of 10−15 mL/h. The column fractions comprising the peak of phosphotransferase activity were pooled and dialyzed overnight against 1 L of buffer B [20 mM KH_2PO_4, 1 mM dithiothreitol (DTT), pH 6.5], centrifuged to remove insoluble material, and applied to a Mono S 5/5 column equilibrated with buffer B. The mutant protein was eluted with a linear gradient of 0−300 mM of KCl in buffer B. Three peaks of phosphotransferase activity were detected; the second and largest peak was used for the studies described below. This corresponds to isoform II which is phosphorylated at S10, T197, and S338 (*7*).

Tryptic Mapping and Mass Spectrometry. The mutant proteins were digested with TPCK-treated trypsin (1:50 w/w) for 16 h. The digested peptides were then resolved by HPLC with a VYDAC C_{18} column (0.46 × 25 cm) and eluted with a mobile phase gradient (5−40% B, 80 min; 45−75% B, 30 min) formed by 10 mM sodium phosphate (pH 6.8; B) and acetonitrile (B). The eluent absorbance was monitored at 219 nm. Sequencing of the peptides was performed by using a gas-phase sequencer with an on-line PTH analyzer (Applied Biosystems, Inc., Models 470A and 120). Mass spectroscopy was performed with a Hewlett-Packard 5998A mass spectrometer with a 5989B electrospray interface.

Fluorescein Maleimide Labeling. The mutant C subunit sample (1−0.5 mg) was initially buffer-exchanged by elution through a G-25 column (1 × 5 cm) equilibrated with buffer C (20 mM MOPS, 50 mM KCl, pH 7.2) The protein fractions were pooled, and the concentration of the pooled sample was determined spectrophotometrically by using an $A^{0.1\%}_{280}$ extinction coefficient of 1.0. In the case of the four X-to-Cys mutant proteins, the native cysteines (C199 and C343) were protected from modification by the addition of ATP (4 mM) and $MgCl_2$ (6 mM) to the reaction mixture (*8*). A 5-fold molar excess of fluorescein maleimide was then added, and the reactions were allowed to proceed for 1 h at room temperature, protected from light. The reaction mixtures were then applied to a Sephacryl S-200 column equilibrated at room temperature with buffer D (20 mM MOPS, 50 mM KCl, 5 mM β-mercaptoethanol, pH 7.2). Fluorescein emission (excitation at 470 nm and emission at 525 nm) from the various column fractions was measured, and the fluorescent fractions with retention times that corresponded to unmodified C subunit were pooled. Aliquots of the concentrated sample were subjected to gel electrophoresis under denaturing conditions (12% SDS−PAGE), and the fluorescent bands were visualized with a mineral lamp to assess

whether any unconjugated fluorescein was noncovalently associated with the labeled-mutant C subunit.

Phosphotransferase Assay. The phosphotransferase activity of the labeled C subunits was quantified by the method of Cook et al. (*9*) with kemptide as a substrate.

Determination of the Stoichiometry of Labeling. The stoichiometry of fluorescein-labeled C subunits was determined spectrophotometrically by substitution of the measured absorbance at 280 (A_{280}) and 490 (A_{490}) nm into the expression:

$$\frac{[\text{fluorescein}]}{[\text{C subunit}]} = \frac{A_{490}/65000}{(A_{280} - 0.18A_{490})/45000} \quad (1)$$

Steady-State Emission Spectra. Steady-state emission spectra were measured using an Instrument S. A., Inc., Jobin Yvon/Spex FluoroMax II spectrofluorometer with the excitation and emission bands set at 5 nm.

Time-Resolved Fluorescence Anisotropy. The time-resolved emission anisotropy was determined by the time-correlated single photon-counting technique (*10*, *11*) with an EEY Scientific nanosecond spectrofluorometer (La Jolla, CA) equipped with an IBH (Edinburgh, U.K.) hydrogen flash lamp. The vertically [$I_{||}(t)$] and horizontally [$I_{\perp}(t)$] polarized emission decays were collected by exciting samples with vertically polarized light while orienting the emission polarizer (Polaroid HNP′B dichroic film) in either a vertical or an orthogonal direction. Excitation and emission bands were selected with Oriel 500 nm short-pass interference (catalog no. 59876) and Corning 3-69 cutoff filters, respectively. Typically, 1×10^4 peak counts were collected (in 5−10 min) for the decays. The total counts in the $I_{||}(t)$ and $I_{\perp}(t)$ curves were scaled with respect to each other by using the steady-state ratio of integrated photon counts/6×10^6 lamp flashes that were detected when the samples were excited with vertically polarized light while the emission polarizer was oriented in either the vertical ($\bar{I}_{||}$) or the horizontal ($\bar{I}_{\perp}$) direction. To minimize convolution artifacts, lamp flash profiles were recorded by removing the emission cutoff filter and monitoring light scatter from a suspension of latex beads. The wavelength-dependent temporal dispersion of the photoelectrons by the photomultiplier (Phillips XP2020Q) was corrected by the data analysis software. The polarization bias (G) of the detection instrumentation was determined by measuring the integrated photon counts/6×10^6 lamp flashes that were detected while the samples are excited with orthogonally polarized light and the emission monitored with a polarizer oriented in the vertical and orthogonal directions.

For vertically polarized exciting light, time-resolved fluorescence anisotropy, $r(t)$, is defined as

$$r(t) = \frac{[I_{||}(t) - GI_{\perp}(t)]}{[I_{||}(t) + 2GI_{\perp}(t)]} \quad (2)$$

The fluorescence lifetimes and correlation times were obtained by simultaneous fitting of the vertical and horizontal emission decay curves from each sample using the Globals Unlimited (Laboratory for Fluorescence Dynamics, Urbana, IL) software package (*12*). Goodness of fit was evaluated from the value of χ^2 and visual inspection of the difference between experimental and an empirical nonassociative model. This model can be expressed as a sum of two exponential expressions:

$$r(t) = r_F \exp(-t/\phi_F) + r_S \exp(-t/\phi_S) \quad (3)$$

where r is the amplitude of the decay associated with the exponential decay and ϕ is the correlation time of the anisotropy decay. The subscripts F and S denote the fast and slow decay processes, respectively. Although the zero time points for the anisotropy decay plots were arbitrarily designated as the time point associated with the flash lamp peak, the deconvolution analysis utilized data points of the emission decay profiles whose values were at least 1% of the maximum peak emission counts and consequently included data points prior to the emission peak.

Steady-State Fluorescence Anisotropy. Values for the steady-state anisotropy ($\langle r \rangle$) of the various samples were calculated with the expression:

$$\langle r \rangle = \frac{\bar{I}_{||} - G\cdot\bar{I}_{\perp}}{\bar{I}_{||} + 2G\bar{I}_{\perp}} \quad (4)$$

RESULTS

Labeling and Characterization of the Five Mutant Proteins. The five mutant proteins were labeled and purified as described under Materials and Methods. Parallel fluorescein maleimide labeling reactions, carried out with wild-type instead of mutant C subunits, produced no detectable labeling (data not shown), strongly suggesting that the native cysteines in the case of the four X-to-Cys mutant proteins were not labeled under the above conditions. The stoichiometry (fluorescein maleimide/mutant C subunit) of labeling of the various mutants ranged between 0.2 and 0.6. The emission spectra (data not shown) of the five mutants in the *open* (buffer only) and *closed* [in the presence of MgATP and PKIα(5−24)] conformations indicate that neither the site of conjugation nor the conformational state of the C subunit had a major effect on the emission wavelength maximum of any of the five conjugates. Each was within 5 nm of one another (513−518 nm). Similarly, the broadness of the various emission spectra (FWMH) did not differ dramatically, being within 5 nm of one another (36−41 nm). The apparent quantum yield of the labeled mutants, on the other hand, was reduced when each conjugate was in the *closed* state. The presence of MgATP and PKIα(5−24) was associated with a reduction in emission from the labeled K16C, K81C, I244C, N326C, and C199A mutants of 22, 40, 21, 11, and 32%, respectively.

This quenching was not associated with a reduction of the emission lifetime of the labeled mutants (see below) and consequently suggested either an indirect or a direct static quenching action of MgATP or PKIα(5−24) on fluorescein emission. Preliminary experiments showed that PKIα(5−24) had no effect on fluorescein emission. Consequently, steady-state and time-resolved emission experiments (data not shown) were performed and indicated that this quenching was largely static in nature and not diffusion-controlled, because while MgATP was a very effective quencher of the steady-state emission (quenching constant = 2540 M^{-1}) it had a relatively small effect on the emission decay kinetics of fluorescein (K_Q = 94 M^{-1}). The static nature of the quenching strongly suggests that the quenching resulted from

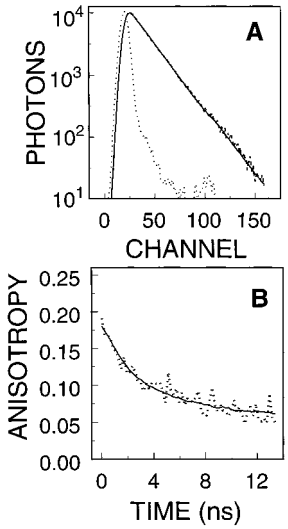

FIGURE 2: Emission and anisotropy decay curves of FM-I244C mutant in the *open* conformation. Panel A illustrates the emission decay (single datum points), a smooth line through these points that was generated with best-fit parameters for a single-exponential equation ($\tau = 4.0$ ns), and a flash lamp profile (dotted line). Here, the emission polarizer was oriented to the magic angle, 55° from vertical, to minimize anisotropic contributions to the observed decay. Panel B illustrates the time-resolved anisotropy decay (single datum points) and a smooth line through these points generated with the best-fit parameters (Table 1) for a double exponential equation (eq 3).

the formation of low-affinity MgATP−fluorescein or ATP−fluorescein complexes. Given that each site of conjugation examined is on the surface of cAPK and that direct interaction of 1 mM MgATP with free fluorescein would have produced a 40% quenching of emission, the MgATP-induced quenching of the fluorescent mutants most likely results from a direct interaction of the MgATP with the conjugated fluorescein. The differences in the MgATP quenching of the labeled mutants probably result from differences in the solvent exposure or in the microenvironment around each conjugation site.

Open Conformation Steady-State and Time-Resolved Anisotropies. The averaged steady-state anisotropy (<*r*>) of the five labeled mutants suggests significant differences in the mobility of the probe associated with each labeling site. The rank order of decreasing <*r*> is FM-K16C (0.145 ± 0.007) ≈ FM-N326C (0.144 ± 0.007) > FM-K81C (0.127 ± 0.002) > FM-I244C (0.111 ± 0.011) ≈ FM-C199A (0.098 ± 0.002). Correcting for the fact that the fluorescence lifetime of FM-K16C is ∼5% shorter than FM-N326C (4.0 versus 4.2 ns), the apparent rank order of increasing mobility of the fluorescein attached to the various mutants is FM-N326C < FM-K16C < FM-K81C < FM-I244C < FM-C199A.

The time-resolved anisotropy decay profiles of the five labeled mutants in buffer (*open* conformation) were fit to a model-free nonassociative biexponential equation (eq 3). In all cases, the fluorescence decay kinetics, a byproduct of the GlobalsUnlimited anisotropy decay analysis, of each labeled mutant were reasonably well fit to a single-exponential decay with lifetimes (τ) that ranged between 4.0 and 4.2 ns (FM-K16C = FM-K81C = FM-I244C = FM-C199A= 4.0 ns; FM-N326C = 4.2 ns). Figure 2A illustrates the emission decay of one of these samples (FM-I244C). The time-resolved anisotropy decay analysis of the labeled mutants yielded, not surprisingly, a somewhat more complex description of the rotational diffusion of the conjugated fluorescein attached to the sites of mutation than provided by the steady-state anisotropy (<*r*>) values (Table 1). The values of the fast rotational correlation time (ϕ_F) ranged between 1.9 and 2.8 ns, with FM-K16C having the lowest value followed by FM-C199A (2.0 ns) and then the other conjugates higher and with essentially comparable values (2.3−2.8 ns; Table 1). The values of the slow rotational correlational time (ϕ_S) did not differ significantly from one another and ranged between 25 and 28 ns (Table 1). These ϕ_S's were in reasonable agreement (given the relative lifetime of the probe and the rotational correlation time of the C subunit) with the rotational correlation time of the free C subunit predicted by the Stokes−Einstein equation (21.3 ns) using the previously published hydrodynamic radius of the C subunit [27.4 Å; (*13*)]. The lack of significant differences in the ϕ_S values would be expected if these values represent the whole-body rotational diffusion of cAPK and if mutation and fluorescein conjugation had no significant effect on whole-body rotational diffusion.

In the absence of any rotational diffusion, the value of r_0 for fluorescein using our instrumentation is 0.34 (data not shown). Observed deviations from the r_0 value of the immobilized fluorophore (r_{VF}) are frequently thought to represent 'very fast' (<ns) angular excursions of the fluorophore that are below the quantification limits of the instrumentation. The variations in the observed r_{VF} values suggest differential amplitudes of these 'very fast' diffusional excursions and are (Table 1) in the decreasing rank order of FM-C199A (0.157) ≈ FM-I244C (0.147) > FM-K81C (0.132) > FM-K16C (0.103) ≈ FM-N326C (0.090). A somewhat different pattern of amplitudes of the 'fast' decay processes (intermediate in frequency between the whole-body and the 'very fast' motions) was observed (Table 1) and is in the decreasing rank order of FM-N326C (0.101) > FM-C199A (0.089) ≈ FM-I244C (0.0.086) > FM-K16C (0.077) > FM-K81C (0.062). The differential pattern of rate and amplitudes of anisotropy decay of the various conjugated mutants suggests underlying differences in the character of the local motions at each site of mutation and conjugation.

Closed Conformation Steady-State and Time-Resolved Anisotropies. With the exception of the FM-K81C mutant, the addition of MgATP and PKIα(5−24) had no detectable effect on the steady-state anisotropy (<*r*>) of the labeled mutants (Table 1). The <*r*> values of FM-K16C, FM-I244C, FM-C199A (with C343 labeled), and FM-N326C in the *closed* state were 0.141 ± 0.004, 0.115 ± 0.011, 0.102 ± 0.001, and 0.143 ± 0.009, respectively. The <*r*> of FM-K81C increased from 0.127 ± 0.002 to 0.140 ± 0.003, indicating that the *closed* conformation is differentially associated with a reduction in the rotational freedom of fluorescein attached to the side chain of the K81C mutant.

Examination of the nondeconvoluted anisotropy decay profiles of the labeled mutants in the presence and absence of MgATP and PKIα(5−24) also indicates that only the FM-K81C mutant (Figure 3) is differentially associated with a reduction in the rotational freedom of the fluorescein attached to the K81C mutant as the C subunit goes from the *open* to the *closed* conformation. The r_F value of FM-K81C decreased from 0.062 to 0.045, and ϕ_F increased from 2.3

Table 1: Summary of the Time-Resolved Fluorescence Anisotropy Decay Fitting Parameters for the Labeled Mutants in the *Open* and *Closed* Conformations[a]

conformation and FM-labeled mutant	r_0[b]	r_{VF}[c]	r_F[d]	ϕ_F[e] (ns)	ϕ_S[f] (ns)	$\langle r \rangle$[g]
open						
FM-K16C	0.237 ± 0.006	0.103	0.077	1.9 ± 0.1	26 ± 1	0.145 ± 0.007
FM-K81C	0.208 ± 0.005	0.132	0.062	2.3 ± 0.1	28 ± 1	0.127 ± 0.002
FM-I244C	0.193 ± 0.031	0.147	0.086	2.8 ± 0.2	27 ± 2	0.111 ± 0.011
FM-N326C	0.250 ± 0.001	0.090	0.101	2.6 ± 0.2	25 ± 1	0.144 ± 0.007
FM-C199A	0.183 ± 0.005	0.157	0.089	2.0 ± 0.1	25 ± 1	0.098 ± 0.002
closed						
FM-K16C	0.236 ± 0.010	0.104	0.075	1.8 ± 0.2	25 ± 1	0.141 ± 0.004
FM-K81C	0.206 ± 0.008	0.134	0.045	3.2 ± 0.4	24 ± 2	0.140 ± 0.003
FM-I244C	0.199 ± 0.036	0.141	0.101	2.8 ± 0.2	25 ± 1	0.115 ± 0.011
FM-N326C	0.253 ± 0.001	0.087	0.094	2.7 ± 0.1	24 ± 1	0.143 ± 0.009
FM-C199A	0.180 ± 0.002	0.157	0.082	2.0 ± 0.1	23 ± 1	0.102 ± 0.001

[a] Anisotropy decays were fit to eq 3 by using the Globals Unlimited Computer Program as described under Materials and Methods. The *open* and *closed* conformations are defined by the absence or presence of MgATP (1 mM) and PKIα(5−24) (5 μM), respectively. The average χ^2 for fitting the data from the various samples to eq 3 and emission decays ranged between 1.5 and 2.6. [b] Anisotropy at time equal zero. [c] The amplitude of the 'very fast' decay process which equals 0.34 minus r_0. The value 0.34 is the experimentally determined r_0 of molecular fluorescein in the absence of rotational diffusion. [d] The amplitude of the 'fast' decay process. [e] Fast rotational correlational time. [f] Slow rotational correlation time. [g] Steady-state anisotropy.

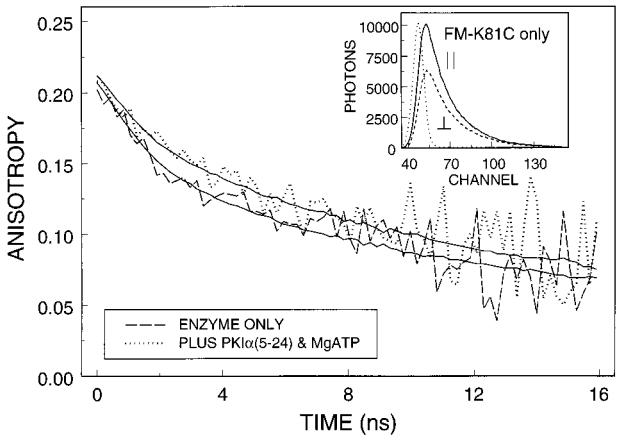

FIGURE 3: Time-resolved fluorescence anisotropy decay of FM-K81C in the *open* and *closed* conformations. The raw (convolved with the excitation lamp) time-resolved fluorescence anisotropy decays of FM-K81C in the *open* (dashed line) and *closed* (dotted line) conformations are shown. The inset shows the excitation lamp pulse (dotted line) and time decay of emissions with the emission polarizer oriented either vertically (||) (solid line) or horizontally (⊥) (dashed line) relative to the vertically polarized excitation beam. The fitting parameters are shown in Table 1. The procedures used to obtain the results and fit the data are described under Materials and Methods. All measurements were performed in MOPS (20 mM), KCl (50 mM), β-mercaptoethanol (5 mM), pH 7.2 at 22 °C. The concentration of the mutants ranged between 100 and 300 nM. The mutants were induced into the *closed* conformation by the addition of 5 mM $MgCl_2$, 1 mM ATP, and 5 μM PKIα(5−24).

± 0.1 to 3.2 ± 0.4 ns, suggesting a decreased fraction and rate of the 'fast' motion of the fluorescein attached to K81C upon the addition of MgATP and PKIα(5−24). The values of r_0, r_{VF}, r_F, ϕ_F, and ϕ_S of the other labeled mutants did not change significantly.

It is of value to note that although a comparison of the *open* and *closed* ϕ_S's shows that the rotational correlation times averaged about 2 ns less when the labeled mutants were in the closed conformation, these changes are within experimental error of the instrument. This is although Olah et al. (*14*) with small-angle X-ray scattering observed that the *closed* conformation has a 9% smaller radius of gyration than the *open* conformation and that with X-ray crystallography calculated that the radius of the *closed* conformation was 1 Å smaller than the *open* conformation (about a 4% reduction in radius) (*2*, *15*). The failure to detect a change in the rotational correlation time here probably reflects (1) the limited sensitivity of this technique when the fluorescent probe has a fluorescence lifetime 5 times less than the rotational correlation time of the macromolecule being measured and (2) the probability that the magnitude of the *open*-to-*closed* volume contraction is closer to that observed by X-ray crystallography (only a 4% reduction in radius) which would, consequently, be more difficult to detect by fluorescence anisotropy with fluorescein as a probe.

DISCUSSION

In this paper, we examined the steady-state and time-resolved emission anisotropy of fluorescein maleimide conjugated to five sites on cAPK in the *open* and in the *closed* conformations. To evaluate these results, it is of value to describe the basic structural features of the sites of conjugation, the crystallographic *B* (or temperature) factors associated with these sites, and also the nature of the molecular dynamics information revealed by fluorescence anisotropy spectroscopy.

Structurally, the K16C site of mutation resides in the N-terminal segment. Several structural, mostly hydrophobic, elements anchor the N-terminal domain to both lobes. In mammalian cells, the first residue of this domain (G1) is myristoylated, and the acyl moiety folds back into a hydrophobic cavity on the large lobe (*1*). The recombinant cAPK used in these studies is not myristoylated, and the first 12 residues are not observed in the X-ray structure, most likely because they are disordered. The K16C site of mutation and labeling is situated on an exposed surface at the beginning of the A helix, and X-ray structural data indicate that the relative position of the residue changes little between the *open* and the *closed* conformations. Although no X-ray structure of the *open* recombinant (nonmyristoylated) cAPK is available, and consequently the backbone flexibility (vibrational displacement and disorder) of this subdomain is unknown, the X-ray crystal structure of the *closed* conformation of the recombinant cAPK has been determined and shows that the main-chain atom *B* factors of K16 and the observed neighboring residues are about 1

Table 2: Relative Main-Chain Atom *B* Factors of the *Open* and *Closed* Conformations of cAPK in the Vicinity of the Sites of Specific Labeling

residues averaged	relative average main-chain atom *B* factors[a]	
	open[b] (Å^2)	*closed*[c] (Å^2)
15−18[d]	31.5[e]	33.7
79−83	33.0	21.0
242−246	28.5	24.2
324−328	na[f]	27.4
327−328	25.1	25.8
341−345	39.0	30.4
whole molecule average (±SD) raw main-chain atom *B* factors	20.2 (±4.3)	29.9 (±10.6)

[a] Because the degree of refinement of the two crystal structures examined differed, it was necessary to normalize the *B* factors so that the two sets of data could be compared. This was calculated by first letting the normalized *B* factors (B_{norm}) for each structure take mean ±SD values of 25 and 7.2, respectively, and then substituting the average main-chain atom *B* factors for each residue (B_i) into the expression: $B_{norm} = [25 + (B_i - B_{avg})/B_{SD}] \times 7.2$ where B_{avg} and B_{SD} are the whole-molecule average and SD for each structure examined. The average (±SD) raw main-chain atom *B* factors for 1CTP (*open*) and for 1ATP (*closed*) are 20.2 ± 4.3 Å^2 and 29.9 ± 10.6 Å^2, respectively. [b] Porcine heart (myristylated) cAPK that was crystallized in the *open* conformation and having a Protein Data Bank (PDB) entry filename of 1CTP (*1*). [c] Murine recombinant cAPK (nonmyristoyled) that was crystallized in the *closed* conformation and having a PDB entry filename of 1ATP (*16*). [d] Only the main-chain atoms of these residues were averaged because residues 1−14 of the *closed* form of cAPK were not observed. [e] This value will probably be lower in the nonmyristoylated form of cAPK because the myristoyl moiety on G1-folds back into a hydrophobic cavity in the large lobe which will probably limit the mobility of the N-terminal domain. [f] Residues 318−326 of the *open* conformation of cAPK are not observed in the crystal structure.

SD above average for the entire peptidyl backbone (Table 2), indicating some disorder at this site.

The N326C site of mutation is positioned in the middle of the C-terminal "tail" which like the N-terminal segment interacts with both lobes. Although residue N326 is not observed in the crystallographic structure, it might be thought that N326 should be disordered in the *open* conformation; however, the averaged main-chain atom *B* factors of the observable adjacent residues (327−330) are low (about average for all the main-chain atoms) and about the same magnitude in both the *open* and *closed* conformations (Table 2). The low *B* factors and therefore low disorder of the residues adjacent to N326 would presumably limit the motion of N326 and suggest that the peptidyl backbone flexibility around N326 is in fact about equal to the average of all the main-chain atom *B* factors, which is to say relatively ordered.

The C343 site of labeling (with the FM-C199A mutant) is very near the end of the C-terminal tail, and based on the main-chain atom *B* factors, this is a relatively flexible segment. The average main-chain atom *B* factors are about 2 SD above the average in the *open* conformation and decrease to 1 SD above average in the *closed* conformation (Table 2). The sites of the K81C and I244C mutations are both exposed and are at the tips of the small and large lobes, respectively. K81C at the C-terminal end of the B helix and I244C at the N-terminal end of the G helix are in regions where the average *B* factors of the main-chain atoms are low and are very similar to one another in the *open* conformation (Table 2). In the *closed* conformation, on the other hand, the *B* factors around K81 decrease by about a 2 SD, and the relative position of this region shifts as much as 8 Å toward the large lobe. This is in contrast to the main-chain atom *B* factors at and around I244 that change little relative to the *open* conformation (Table 2).

Time-resolved fluorescence anisotropy allows the direct monitoring of the reorientation of the emission transition dipole moment of a fluorophore in the picosecond/nanosecond time domain. When the fluorophore is conjugated to peptidyl side chains, as is the case here, the motion of the fluorophore is obviously influenced by both global and local movements. Although the influence of the global or whole-body motions of the protein on the fluorophore is the same no matter where the fluorophore is located, the motions of the fluorophore tether arm, cysteine side chain to which the fluorophore is conjugated, and the α-carbonyl backbone in the region of the conjugated fluorophore, of course, vary with the site of conjugation. A major difficulty in the use of fluorescence anisotropy to assess global and local protein dynamics is the assignment of the anisotropy decay parameters to specific dynamic elements. With this said, the rate of the slow anisotropy decay process (ϕ_S) is probably the easiest to assign. It can reasonably be attributed to whole-body rotation diffusion, because its observed value is close to the value predicted by the Stokes−Einstein equation for a protein the size of cAPK (21.5 ns).

The r_{VF}, r_F, and ϕ_F parameters are more difficult to assign. If tether arm and side chain motions are largely unhindered by neighboring groups, as is usually the case for exposed surface residues such as the sites of labeling studied here, then their rotational correlational times should occur in the subnanosecond time domain. Thus, the very fast motions would primarily influence the values of r_{VF} and not r_F, ϕ_F, or ϕ_S which are associated with nanosecond dynamics of the samples examined here. On the other hand, diffusional processes that occur in the low nanosecond time domain such as small-scale peptidyl segmental motions might be expected to influence the observed values of the r_F or ϕ_F . And indeed, to some degree this can be seen in an examination of the correlation between the average main-chain atom *B* factors of small segments (±2 residues) around each site of conjugation and the observed r_F, ϕ_F, and r_{VF} values for the various specifically labeled mutants in the *open* and *closed* conformations (Figure 4). The ϕ_F values are strongly correlated ($r = -0.87$) with the averaged main-chain atom *B* factors of the residues around each site of conjugation, and very weakly if at all correlated with r_{VF} ($r = 0.11$) and r_F ($r = 0.32$).

Why there is a strong correlation between the rate of the fast anisotropy decay process (ϕ_F) and the main-chain atom *B* factors is not completely clear. However, in part, it occurs because *B* factor averaging was performed on segments of the main-chain atom residues and not single atoms or residues. The rate of the fast anisotropy decay is a composite of motional processes that are occurring on the low nanosecond time scale. The *B* factor for an atom is a Gaussian probability distribution for finding that atom in a particular point in space at any particular time. It therefore includes all effects of thermal motion, of disorder in the crystal, and of errors in the model. The actual thermal oscillation about the equilibrium position of an atom is typically on the

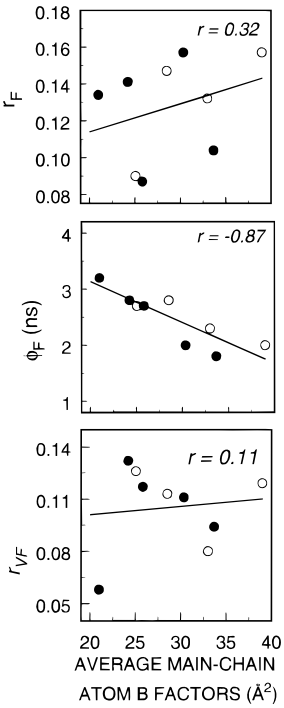

FIGURE 4: Relationship between averaged main-chain atom *B* factors around each site of labeling and r_{VF}, r_F, and ϕ_F. The anisotropy measurements of r_{VF}, r_F, and ϕ_F were taken with the labeled mutants in either the *open* (unfilled circles) or *closed* (filled circles) conformations of cAPK.

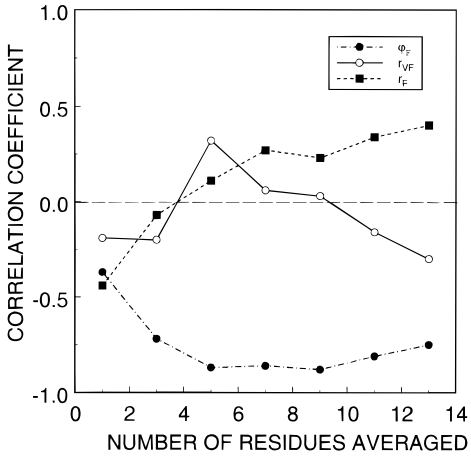

FIGURE 5: Relationship between the number of residues used in the calculation of the averaged main-chain atom *B* factors and the correlation between these averaged *B* factors and r_{VF}, r_F, and ϕ_F. Unfilled circles, r_{VF}; filled circles, ϕ_F; filled squares; r_F.

femtosecond time scale, while peptidyl backbone motions are on the pico- to microsecond time scale. When only the main-chain atoms of the labeled residue are correlated to ϕ_F, the correlation between ϕ_F and the main-chain atom *B* factors is low ($r = -0.37$) but increases to -0.72 when the averaging includes one residue on each side of the labeled residue and reaches a maximum value (-0.88) when the averaging includes four residues on each side of the labeled residue (Figure 5). Averaging the *B* factors of more than four residues before and after the site of labeling is associated with a slowly decreasing correlation between ϕ_F and the main-chain atom *B* factors (Figure 5), suggesting again that the ϕ_F parameter is sensitive to the backbone flexibility of the short segments around each site of labeling.

If ϕ_F is a measure of the flexibility of short peptidyl segments around the sites of conjugation, then several conclusions can be drawn about (nanosecond time domain) the peptidyl backbone flexibility of the various subdomains of the C subunit in both the *open* and the *closed* conformations. First, in the *open* conformation, the fluctuations of the α-carbonyl backbone motions are faster around K16 near the N-terminus and C343 near the C-terminus than around K81, I244, or N326, which are essentially equal to one another. Of the areas examined, only the segmental flexibility around K81 measurably changed upon pseudosubstrate-induced closure of the interdomain cleft that forms the active site. Here, only the rates of nanosecond motions were measurably reduced upon transformation into the closed conformation. Curiously, the addition of PKIα(5−24) and MgATP had no significant effect on the fast rotational correlation time associated with FM-C199A (C343 labeled) when the *B* factors around C343 are reduced by about 1 SD upon conversion to the *closed* conformation. This failure to detect a significant change in the mobility of fluorescein attached to C343 may suggest that the *open*-to-*closed* reduction of the *B* factors around C343 is associated more with >15 ns diffusion and therefore appears as static order on the low nanosecond time scale.

Two final comments: First, with the exception of FM-K81C results, the steady-state anisotropy values were poorly correlated to the main-chain atom *B* factors around each site of labeling. Consequently caution must be used in linking any changes in the steady-state anisotropy of fluorophore conjugates to changes in backbone flexibility. Second, the terms *open* and *closed* conformations require additional clarification. In this paper, we have used these terms somewhat loosely by implying that they represent two discreet conformations when in fact the situation is more complicated. The cAPK C subunit is probably in equilibrium between many conformational states (*2*). In the presence of MgATP and PKIα(5−24), this equilibrium strongly favors a contracted (*closed*) conformation. This *closed* conformation is well-defined by its X-ray crystallographic structure and represents an absolute limit of the contracted state. The *open* conformation, however, is more likely to be a mixture of conformations in dynamic equilibrium with each other. Some of these conformations may be more expanded than revealed by the published *open* state crystallographic structures (*16*). With this in mind and with the fact that closing of the interdomain active-site cleft involves subdomain displacements primarily within the small lobe (*3*), it is not surprising that the largest PKIα(5−24)/MgATP-induced change in backbone flexibility is observed when the fluorescein is attached to residue 81 in the B helix of the small lobe.

In summary, we examined the correlation between the various anisotropy decay parameters from five specifically labeled mutants with the average main-chain atom *B* factors around each site of labeling and with the theoretical rotational correlation time of cAPK. The observed slow rotational time (ϕ_S) was reasonably well correlated with the predicted whole-body rotational correlation time; however, the 5−9% change in the radius of the C subunit associated substrate/pseudosubstrate-induced volume contraction could not be unambiguously detected. Significantly, the observed fast rotational correlation time (ϕ_F) of the anisotropy decay was inversely

proportional to the small segments of the main-chain atom *B* factors around each site of conjugation, suggesting that site-directed fluorescent labeling and time-resolved anisotropy provide an alternative low-resolution approach to measure peptidyl backbone dynamics. Finally, of the sites examined, only the area around K81 in the small lobe was measurably affected by substrate/pseudosubstrate-induced contraction; the rates of the peptidyl segmental motions were reduced.

ACKNOWLEDGMENT

We thank Dr. Lynn Ten Eyck for helpful discussions on *B* factors.

REFERENCES

1. Zheng, J., Knighton, D. R., Xuong, N. H., Taylor, S. S., Sowadski, J. M., and Ten Eyck, L. F. (1993) *Protein Sci. 2*, 1559−1573.
2. Narayana, N., Cox, S., Xuong, N., Ten Eyck, L. F., and Taylor, S. S. (1997) *Structure 5*, 921−934.
3. Cox, S., Radzio-Andzeim, E., and Taylor, S. S. (1994) *Curr. Opin. Struct. Biol. 4*, 893−901.
4. Slice, L. W., and Taylor, S. S. (1989) *J. Biol. Chem. 264*, 20940−20946.
5. Kunkel, T. A. (1985) *Proc. Natl. Acad. Sci. U.S.A 82*, 488−492.
6. Lew, J., Coruh, N., Tsigelny, I., Garrod, S., and Taylor, S. S. (1997) *J. Biol. Chem. 272*, 1507−1513.
7. Hemmer, W., McGlone, M., and Taylor, S. S. (1997) *Anal. Biochem. 245*, 115−122.
8. First, E. A., and Taylor, S. S. (1989) *Biochemistry 28*, 3598−3605.
9. Cook, P. F., Neville, M. E., Jr., Varana, K. E., Hartl, F. T., and Roskoski, R. Jr. (1982) *Biochemistry 21*, 5794−5799.
10. Yguerabide, J. (1972) *Methods Enzymol. 26*, 498−578.
11. Hanson, D. C., Yguerabide, J., and Schumaker, V. N. (1981) *Biochemistry 20*, 6842−6852.
12. Beechem, J. M., Gratton, E., Ameloot, M., Knutson, J. R., and Brand, L. (1991) in *Topics in Fluorescence Spectroscopy* (Lakowicz, J. R., Ed.) Vol. 2, pp 241−305, Plenum Press, New York.
13. Herberg, F. W., Dostman, W. R. G., Zorn, M., Davis, S. J., and Taylor, S. S. (1994)
14. Olah, G. A., Mitchell, R. D., Sosnick, T. R., Walsh, D. A., and Trewhella, J. (1993) *Biochemistry 32*, 3649−3657.
15. Narayana, N., Cox, S., Shaltiel, S., Taylor, S. S., and Xuong, N. (1997) *Biochemistry 36*, 4438−4448.
16. Karlsson, R., Zheng, J., Xuong, N., Taylor, S. S., and Sowadski, J. M. (1993) *Acta Crystallogr. D49*, 381−388.

BI980560Z